Engineering Failure Analysis 192 (2026) 110817

Contents lists available at ScienceDirect

Engineering Failure Analysis

journal homepage: www.elsevier.com/locate/engfailanal

Root cause analysis and Resolution of a brass extrusion mandrel failure

M. Schmidt [a], D. Migliorino [a], L. Buglioni [b], G. Abate [b], D.Martínez Krahmer [a,b], L.N.López de Lacalle [c,*], A.Sánchez Egea [d]

[a] Instituto de Tecnología e Ingeniería, Universidad Nacional de Hurlingham (UNaHur), Buenos Aires, Argentina
[b] Centro de Mecánica, Instituto Nacional de Tecnología Industrial (INTI), Buenos Aires, Argentina
[c] Department of Mechanical Engineering, Escuela de Ingeniería de Bilbao, Universidad del País Vasco, Bilbao 48013, Spain
[d] Departament d'Enginyeria Mecànica, Universitat Politècnica de Catalunya, Catalunya, Spain

ARTICLE INFO

Keywords:
Engineering failure analysis
Hot extrusion
Mandrel
Fractography
Finite element method
Deep-hole drilling
Gun drilling

ABSTRACT

Mandrels made of DIN 1.2367 (AISI *H*10) hot-work tool steel are critical components in the hot extrusion of seamless C27000/C38500 brass tubes. In this case, after a change in the tooling supplier, mandrel life dropped to ~ 10% of the historical benchmark, with premature brittle fractures occurring during routine production. A comprehensive failure investigation was performed combining chemical composition verification (ASTM E415), tensile testing (ASTM E8), hardness mapping (ASTM E18), surface roughness measurements, Charpy impact testing (ASTM E23), fractographic examination of fracture surfaces, and finite-element simulations of the extrusion stage. The steel chemistry complied with DIN 1.2367; however, the hardness in the upper region exceeded the specified range, consistent with reduced toughness. Fractography showed crack initiation at the inner surface of the cooling channel, where drilling-induced surface damage (e.g., high roughness, burrs, and potential microcracking) served as critical stress concentrators within a region exhibiting hardness gradients. FEM confirmed that this bore is subjected to high axial tensile stresses during extrusion, particularly for the current die geometry. Corrective actions targeted the channel surface quality by replacing conventional twist drilling with carbide-tipped gun drilling, thereby removing critical defects and producing a uniform internal finish. After implementation, mandrel service life returned to the original level (~250 pressings), restoring process reliability and reducing unplanned downtime.

1. Introduction

Extrusion processes, which are fundamental for the manufacturing of seamless metallic components, have experienced sustained industrial growth in recent decades [1]. In seamless tube forming, two major routes are commonly distinguished: the Mannesmann process and direct extrusion with a mandrel [2]. These and other hot forming processes (e.g., forging) require large and high-cost equipment; consequently, many companies operate a single production line. The failure of a critical tool—or, in the worst case, the main press—may therefore lead to substantial losses due to unplanned downtime [3].

Failure analysis of extrusion tooling and mandrels in particular requires an integrated approach linking several bodies of

* Corresponding author.
E-mail address: norberto.lzlacalle@ehu.eus (L.N.López de Lacalle).

https://doi.org/10.1016/j.engfailanal.2026.110817
Received 23 December 2025; Received in revised form 24 March 2026; Accepted 26 March 2026
Available online 27 March 2026

knowledge in the specialized literature. Systematic reviews help to contextualize the state of the art, identifying advances, methodological limitations and underexplored areas. For example, Leśniak et al. [4] reviewed recent developments in extrusion of aluminum and magnesium alloys, covering die design, coatings and emerging technologies. Qamar et al. [5] identified main die defects, their causes and corrective actions. Schwartz et al. [6,7] showed that replacing H13 with Inconel 718 in copper extrusion can markedly increase die life. Arif et al. [8] analyzed 616 die failures in aluminum extrusion and reported fatigue fracture (46%), wear (26%) and plastic deformation (19%) as dominant modes.

Beyond die-focused studies, Behrens and Yilkiran [9] emphasized that hot forming tools generally fail due to combined thermal, mechanical and tribological loads; treatments such as nitriding and hard coatings are key to improve durability. Tseronis et al. [10] attributed premature fracture of an H13 die to a combination of geometric asymmetry, manufacturing defects and inadequate nitriding. Gasem [11], studying an H13 mandrel for aluminum extrusion, showed that multiple gas-nitriding cycles can generate a brittle layer that promotes crack initiation.

From a tribological standpoint, Zhao et al. [12] investigated the wear of typical die materials (H13, YG8, and CVD coatings) at 500 °C and identified adhesion, abrasion, and fatigue as the dominant mechanisms. Thewes et al. [13] observed strong copper adhesion on uncoated dies and concluded that surface modification (e.g., boriding) can significantly mitigate it. Liu et al. [14] found adhesive friction to be the main component of flow resistance in extrusion of Al–Mg–Si–Cu alloys.

To predict stresses and failure, finite element modeling (FEM) has been widely used. Akhtar and Arif [15] implemented fatigue damage models in FEM to predict the life of aluminum dies, showing that the Morrow model reproduces observed failures. Gattmah et al. [16] and Jing et al. [17] analyzed the influence of friction, temperature, and geometry on extrusion loads and stresses, validating their results against experiments. Lin et al. [18] proposed die-profile optimization to improve load distribution, and Ahmed et al. [19] used FEM to study early failures due to plastic deformation and to identify optimal operating conditions. Experimental validation has complemented these numerical approaches [20,21].

Despite abundant literature on die failures—especially in light-metal extrusion—studies focusing on mandrel failures are limited [22]. This work showed the importance of structural insufficiencies, particularly under surface area and their role in the failure of flow forming tooling, and metallurgical defects were related in [23]. In particular, no prior work has addressed mandrel failures in brass extrusion, highlighting a significant gap. In addition to solving an industrial problem, this absence further motivates the present study, which aims to characterize and resolve recurrent mandrel fractures.

In summary, premature fracture of critical components in manufacturing processes is an important issue in the metallurgical industry due to its economic impact and the risk to operational continuity. Here, recurrent failures of DIN 1.2367 (AISI *H*10) mandrels used in hot extrusion of C27000 and C38500 brass tubes are analyzed after a drastic drop in service life. The work integrates mechanical testing, fractography, and FEM to identify the root cause and validate an effective corrective machining strategy.

2. Problem Description

Following a change in the tooling supplier, a significant reduction in the service life of mandrels used for the hot extrusion of seamless tubes was observed. Mandrels from the new batches exhibited brittle fracture during forming, failing to meet the previously established durability criterion (see Fig. 1).

In this context, the mandrels were subjected to differential heat treatment to achieve a controlled hardness gradient along their length. First, a homogeneous quenching treatment was applied, consisting of austenitization at 1130 °C followed by forced air cooling, with the mandrel positioned vertically to ensure uniform cooling conditions. Subsequently, a global tempering treatment was performed on the entire component using a double tempering cycle in a molten-salt bath at 550 °C, resulting in a bulk hardness of approximately 50 HRC. Finally, a localized secondary tempering was applied to the working upper zone (approximately 230 mm in length) by partial immersion of the vertically oriented mandrel in a molten-salt bath at 640 °C, reducing the hardness in this zone to approximately 40 HRC. The intermediate region exhibited a smooth hardness transition due to the thermal gradient generated during the localized tempering stage. This heat treatment route is consistent with the procedures reported by N. Wilda et al. for AISI H-series hot-work tool steels [24]. Whereas typical life is about ∼ 250 pressing cycles, the premature failures occurred after approximately 10% of this expected value. Failures were concentrated in the transition zone between the upper and lower sections of the mandrels, as

Fig. 1. Examples of brass-tube extrusion mandrels failed by brittle fracture.

shown in Fig. 2. In the two representative cases analyzed (mandrels A and B), the fracture surface was located at 234 ± 8 mm from the mandrel support face. Although such deviations can fall within the expected range of fatigue scatter, evidence suggests these failures were driven by surface topography rather than bulk material defects. Localized surface roughness acted as a stress concentrator, increasing the probability of crack initiation. Subsequent improvements to the surface finish significantly mitigated the fatigue risk, confirming that surface quality is a critical parameter for operational life. Finally, billets are cylindrical, and during the first stage of extrusion, the mandrel pierces the billet through the thickness to establish the internal tube diameter.

3. Methodology

The methodology followed a sequential workflow. First, compliance with mandrel requirements was checked through chemical composition analysis, mechanical property testing and hardness measurements. Fig. 2 shows the manufacturing drawing (reproduced from the original) of the mandrel used for hot extrusion of brass tubes. The specified material is the DIN 1.2367 hot-work tool steel. To verify compliance of the failed mandrels A and B (same manufacturing batch), chemical analyses were performed by optical emission spectrometry using an Espectrotest TAG No. MM 361, following ASTM E415. Table 1 reports the nominal composition range for DIN 1.2367 and the measured values for mandrels A and B.

For mechanical properties and hardness tests, the mandrels were divided into upper and lower zones. Tensile specimens were machined by turning from longitudinal samples taken from the wall thickness of the upper zone. Specimens corresponded to ASTM E8 'specimen 2′ geometry and were tested on an Emic tension–compression machine (TAG No. MM 203). Yield strength (Y), ultimate tensile strength (Rm) and elongation at fracture (A%) were obtained. Table 2 lists the required room-temperature strength values for the upper and lower zones, along with the measured values for the upper-zone specimens.Hardness was measured on the Rockwell C scale using a Petri hardness tester (TAG No. MM-12) following ASTM E18.

As a second experimental phase, additional analyses were performed: surface roughness measurements, Charpy impact testing, and fractographic analysis of fracture surfaces. Arithmetic mean roughness (Ra) was measured on the external diameter along the longitudinal direction using a Surftest SJ-210 profilometer (cut-off $Lc = 0.8$ mm; evaluation length $Ln = 4$ mm). Charpy V-notch specimens (10 × 10 × 55 mm) were extracted longitudinally from both upper and lower zones and tested at room temperature (23 °C) per ASTM E23 using an Amsler pendulum (TAG No. MM-010). Fractography was performed from images of the fractured cross-sections.

Finally, finite element simulations had two objectives: (i) determine the stress state experienced by the mandrel under standard process conditions; and (ii) through a design of experiments (DOE), assess geometric factors of the extrusion tooling (die angle, die radius, and mandrel taper angle) that could significantly influence extrusion load and mandrel stresses and thus guide future improvements. The hot extrusion process for C38500 brass tubes was simulated using the open-source OpenRadioss software. The experimental setup involved a billet measuring 170 mm in diameter and 375 mm in length, housed within a container with an internal diameter of 175 mm, an external diameter of 702 mm, and a length of 750 mm. Regarding thermal conditions, the billet was heated to a furnace exit temperature of 840 °C, while the container, mandrel, and die were maintained at 200 °C. Friction parameters were modeled following the approach of Ying et al. [17]. In the model, the mandrel is assumed to exhibit purely elastic behavior during extrusion. Finally, the study employed a Design of Experiments (DOE) with a full factorial design comprising three factors at two levels, as detailed in Table 3.

Four die geometries were evaluated (ID = 70 mm): R2/AM90, R5/AM90, R2/AM60 and R5/AM60; and two mandrel tapers: AP0.03 and AP0.09.

4. Results and Discussion

Based on the chemical composition results (Table 1), mandrels A and B fall within the specified range for DIN 1.2367 steel. Tensile-test results (Table 2) indicate ultimate tensile strength values that are, on average, 8.2% higher than the maximum required value.

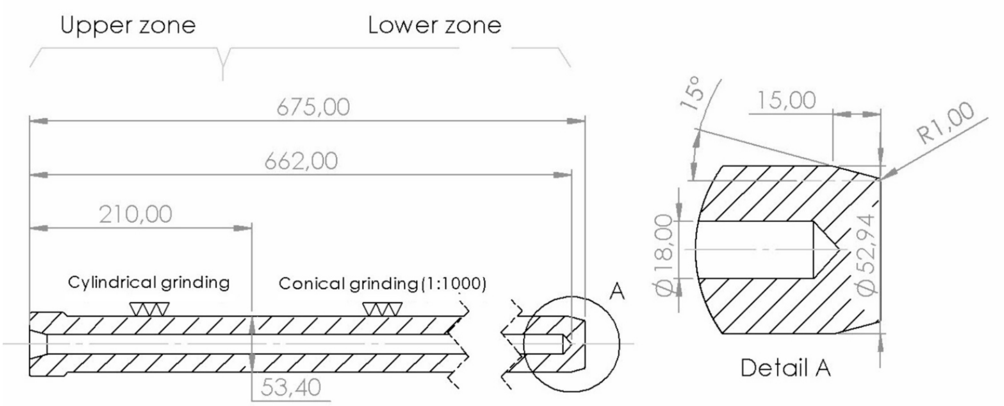

Fig. 2. Manufacturing drawing of the hot brass-tube extrusion mandrel (DIN 1.2367).

Table 1
Chemical composition (wt%) of DIN 1.2367 steel (nominal) and mandrels A and B.

Element	Nominal (wt%)	Mandrel A (wt%)	Mandrel B (wt%)
C	0.35–0.40	0.37	0.37
Mn	0.30–0.60	0.35	0.35
Si	0.30–0.50	0.31	0.28
P	Max. 0.03	0.021	0.023
S	Max. 0.03	0.008	0.008
Cr	4.70–5.20	4.85	4.87
Mo	2.70–3.30	2.91	2.92
V	0.40–0.70	0.66	0.68

Table 2
Mandrel mechanical properties: requirements and measured values.

Zone	Requirement Rm (MPa)*	Mandrel A	Mandrel B
Upper	1275–1324	Y = 1220 MPa Rm = 1426 MPa A = 9.5%	Y = 1223 MPa Rm = 1439 MPa A = 10.3%
Lower	1618–1716	—	—

* Note: tensile tests were performed only on specimens extracted from the upper zone because fractures occurred there.

Table 3
Factors and levels used in the factorial DOE.

Factor	Level 1	Level 2
Die angle (°)	60	90
Die radius (mm)	2	5
Mandrel taper angle (°)	0.03	0.09

Note: the die currently used in the plant has a 90° angle and a 5 mm radius; the theoretical taper of the mandrel is ~ 0.0573°.

Hardness results are shown in Table 4. Both samples exhibited upper-zone hardness values that are, on average, 10.4% higher than the maximum allowable value; in mandrel B, lower-zone hardness also exceeded the upper limit by ~ 2.5%. These findings, together with tensile test results, indicate reduced toughness and therefore greater susceptibility to service fracture. External cylindrical grinding resulted in Ra values (0.44 ± 0.06 μm) within the typical range reported for cylindrical grinding of hardened steels (0.30–1.00 μm) [25] (Table 5), indicating adequate control of the external surface finish.

Charpy impact results at room temperature (23 °C) are listed in Table 6. The absorbed energy is consistently higher in the upper zone than in the lower zone, suggesting reduced toughness toward the lower region and a significant mechanical gradient along the tool. As a reference, Qamar [26] reported that values near 10 J are close to the lower acceptable limit for quenched-and-tempered *H*11-type steels. Fig. 3 presents the fractographic assessment of the fracture sections, which indicates crack initiation at the inner diameter, suggesting fatigue-assisted fracture driven by stress concentrations. In both mandrels, fracture initiated at the cooling-channel bore, consistent with cyclic stress concentration and/or pre-existing surface defects or microcracks. Accordingly, FEM was used to further investigate the load and stress state acting on the mandrel during extrusion.

Fig. 4 shows a magnified view of the initial crack area, enhanced to highlight the failure mechanisms. The analysis focuses specifically on the initiation of microcracks, which appear to originate from localized surface points or zones. The irradiation shape in Fig. 4 right is clear. There in no any Herzian contact here, defects were located stating in surface defects due the lack of smoothness.

Following crack penetration, small-scale spalling occurs. As illustrated in Fig. 4 left, the process begins at the origin and leads to subsequent shearing under surface crack failure. Both cases demonstrate consistent morphological features. In Fig. 4 right, a hand fan pattern typical of surface cracks is clearly defined. There is not hertzian contact in those points, so undersurface shear stress cannot be the cause.

The extrusion loads predicted by the FEM simulations for all DOE combinations are summarized in Fig. 5. The results confirm that the configuration currently implemented in the plant—characterized by a die angle of 90° and a small die radius—yields among the

Table 4
Rockwell hardness (HRC) requirements and measured values.

Zone	Requirements (HRC)**	Mandrel A	Mandrel B
Upper	38.5–40.0	44.0 ± 1.0	44.3 ± 0.6
Lower	49.0–52.0	50.7 ± 0.6	53.3 ± 0.6

** HRC values were obtained by dividing the tensile strength from Table 2 by 33, using the correlation between Rm (MPa) and HRC for quenched-and-tempered tool steels [22].

Table 5
External diameter surface roughness (Ra) for mandrels A and B.

Sample	Reference Ra (μm) [23]	Measured Ra (μm)
A and B	0.30–1.00	0.44 ± 0.06

Table 6
Charpy absorbed energy (J) at 23 °C by zone and mandrel.

Zone	Mandrel A (J)	Mandrel B (J)
Upper	16.0 ± 2.0	18.7 ± 1.2
Lower	12.0 ± 2.0	10.0 ± 2.0

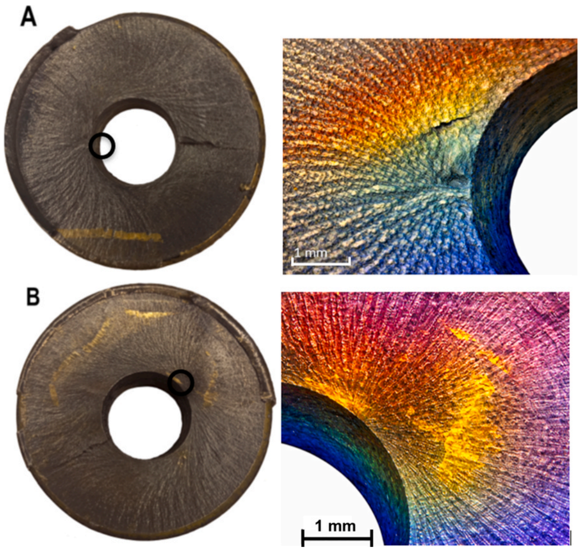

Fig. 3. Fracture surfaces of mandrels A and B: circles indicate crack initiation sites, with high-magnification insets showing characteristic topographic details.

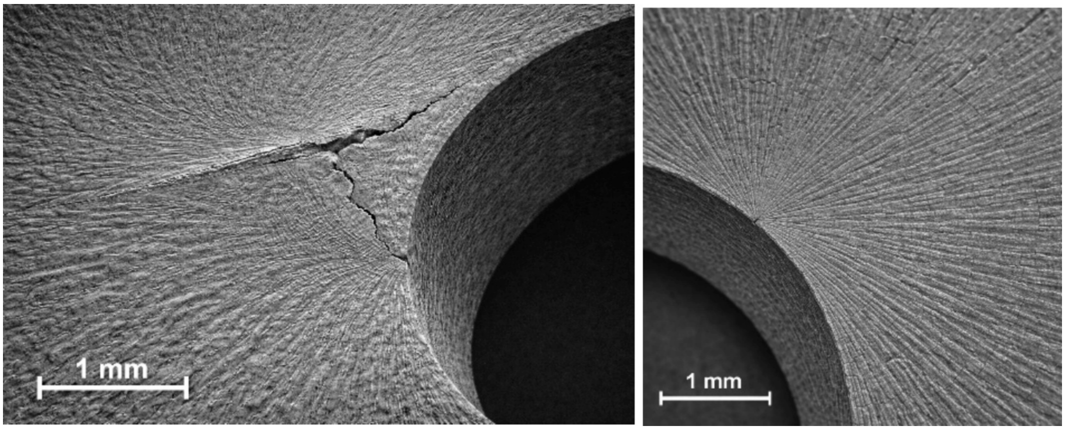

Fig. 4. A more detailed examination of cracked stating areas: left) mandrel A, and right) mandrel B.

highest extrusion loads, consistently exceeding 700 t. The boxplots clearly identify the die angle as the dominant factor affecting the process; transitioning from a 90° to a 60° configuration results in a substantial reduction in load, with the 60° setup yielding the lowest recorded values, often falling below 625 t. In contrast, variations in die radius (from 2 to 5 mm) and mandrel angle (from 0.03 to 0.09) exhibit a negligible influence on the extrusion load, as the median values remain nearly constant across their respective parameter ranges.

The radial stress distributions illustrated in Fig. 6 characterize the internal mechanical state of the mandrel under various geometric

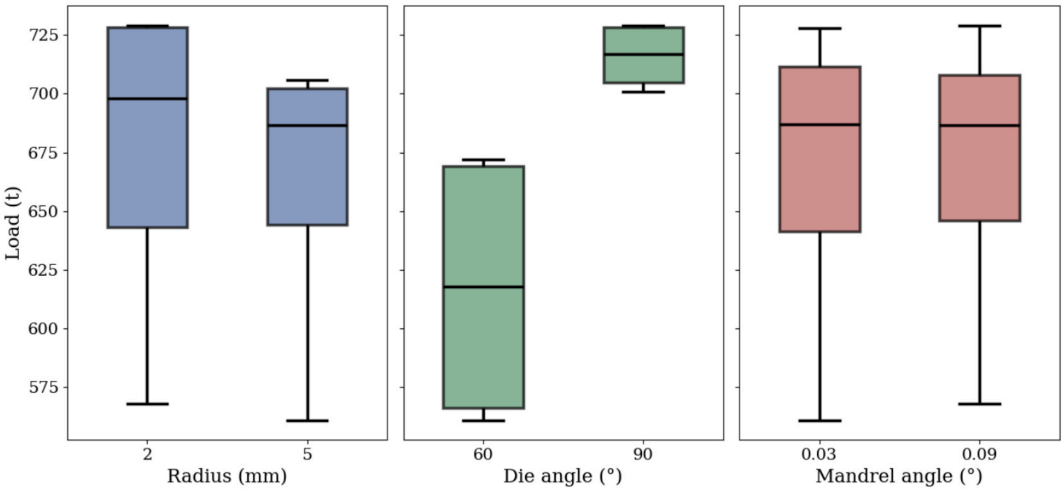

Fig. 5. Boxplots of extrusion load vs. DOE factors and levels.

configurations. Across all eight simulated conditions, combining fillet radii (R_2,R_5), mandrel angles (AM60, AM90), and aperture sizes (AP0.03, AP0.09), the results indicate low-magnitude compressive stresses in the vicinity of the cooling-channel bore. These compressive values remain relatively stable, typically ranging between $-2.0x10^{-8}$ and $-2.7x10^{-8}$ Pa. Notably, the figure demonstrates minimal sensitivity to geometric variations; the blue-toned compressive zones consistently localize within the central regions regardless of changes in taper angle or aperture depth. This stability suggests that radial loading is dominated by the internal pressure of the extrusion process rather than the external mandrel profile. In contrast, the axial stress distributions in Fig. 6 reveal pronounced tensile stresses concentrated at the cooling-channel bore, which increase significantly with the larger die angle (AM90). These tensile stresses are particularly critical because the mandrel operates at elevated temperatures, where hot-work tool steels such as $H11$ undergo substantial reductions in mechanical strength [27].

Given that (i) fractography identified failure initiation at the cooling-channel bore, (ii) the conventional drilling process used a high-speed-steel twist drill, known to produce poorer internal finishes with pronounced grooves [28], and (iii) FEM predicted high axial tensile stresses at the bore, the drilling process was identified as a key controllable contributor to premature failure. The influence of geometric design parameters on these critical stress states is detailed in Fig. 7, which presents the FEM axial stress maps and their corresponding maximum values for the various Design of Experiments (DOE) combinations. Consequently, based on the high stress concentrations observed in these maps, the cooling-channel drilling operation was modified to mitigate failure risk..

The corrective action implemented replaced the conventional high-speed steel twist drilling process with deep-hole gun drilling using a carbide-tipped drill (grade $H10$, submicrograin structure with a 10% Co binder). This class of tools is well known for producing high-quality deep holes with low, consistent surface roughness, typically Ra = 0.80–1.25 μm [29], which is particularly advantageous for fatigue- and fracture-critical components. Comparative trials were conducted between the previously used multi-pass HSS (M2) drilling process and the proposed gun drilling approach. Internal surface roughness was measured over 100 mm of the hole length to assess both average roughness and depth variability. From a mechanical perspective, the localized grooves and roughness associated with conventional drilling act as micro-notches, generating significant stress concentrations. While such concentrations can theoretically increase local stresses by a factor of 4 to 10, these values are difficult to measure experimentally. Furthermore, current computational models face limitations in accounting for the stochastic effects of small-scale microroughness. In this context, surface roughness acts as a primary accelerator of crack initiation and early growth. Notably, as shown in the axial stress, the macroscopic curvature of the cooling-channel bore is not sufficiently sharp to justify these premature failures; therefore, the microscopic surface topology is the dominant driver of the increased stress state.

Fig. 8 shows that gun drilling produced significantly lower roughness values and a markedly more uniform surface finish along the drilled length. In contrast, HSS drilling produced higher roughness levels and substantially greater scatter, with a clear tendency for roughness to increase with drilling depth. Extrapolation of the roughness–depth trend observed for HSS drilling suggests that, at the fracture location (234 ± 8 mm from the entry), the surface roughness could reach values of approximately Ra ≈ 6 μm. Such roughness levels are expected to act as pronounced stress concentrators, thereby exacerbating the tensile stress state identified at the cooling-channel bore and promoting crack initiation.

Accordingly, the drilling process was permanently modified to carbide-tipped gun drilling. In parallel, the region exhibiting differential mechanical properties associated with the upper–lower transition of the mandrel was eliminated, further reducing the likelihood of localized stress amplification. Following the implementation of these corrective actions and the reintroduction of the modified mandrels into production, mandrel service life was restored to its historical level of approximately 250 pressings, thereby confirming the effectiveness of the measures adopted.

Based on these findings, the drilling process was permanently modified to carbide-tipped gun drilling. This transition was justified by the experimental results in Table 5, in which the measured surface roughness (Ra) was maintained at 0.44 ± 0.06 μm, which is

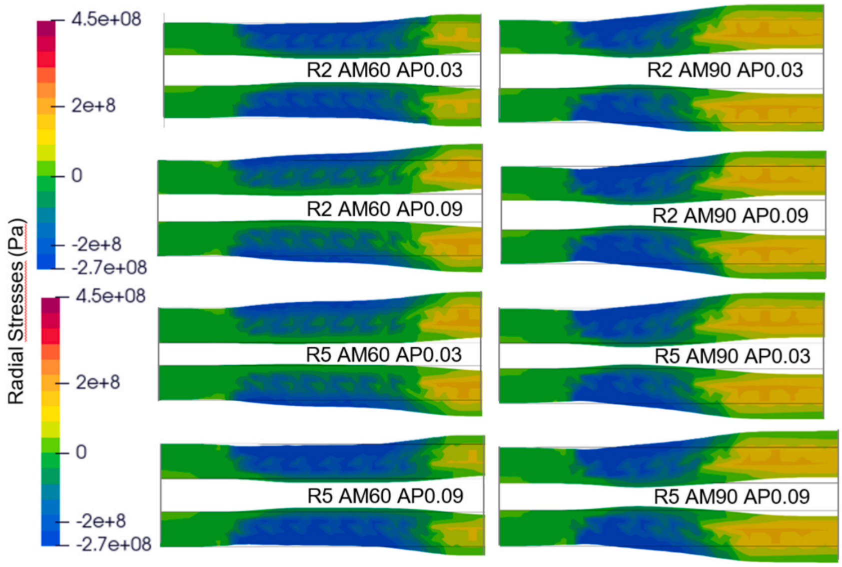

Fig. 6. FEM radial stress maps for the DOE combinations.

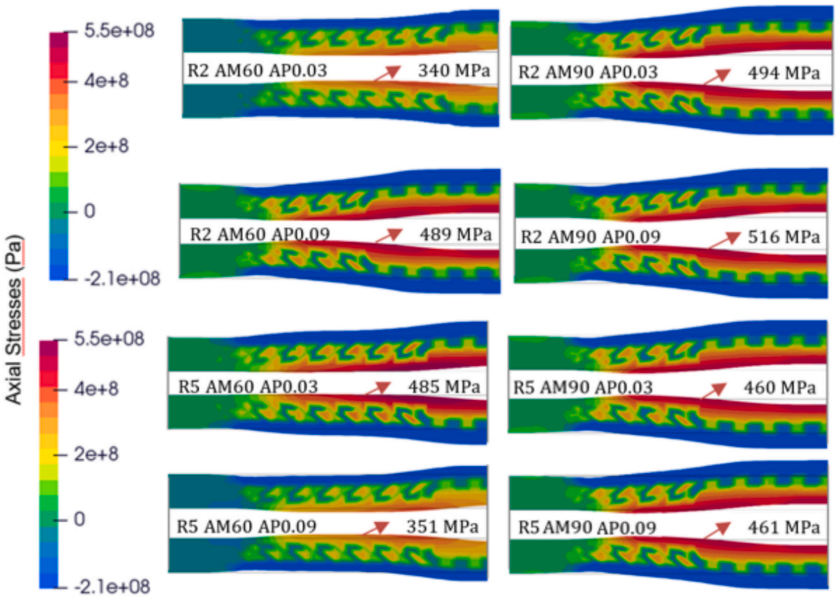

Fig. 7. FEM axial stress maps and their maximums for the DOE combinations.

within the reference range of 0.30–1.00 μm. This improved surface finish significantly reduces the presence of micro-notches that act as crack initiation sites. In parallel, the region exhibiting differential mechanical properties associated with the upper–lower transition of the mandrel was eliminated to prevent localized stress amplification (uniform total hardness of 50 HRC). The critical nature of this transition was evidenced by the mechanical gradient shown in Table 4, where hardness values reached 53.3 ± 0.6 HRC in the lower zone of Mandrel B, exceeding the specified requirements. Furthermore, the toughness analysis in Table 6 revealed a significant reduction in Charpy absorbed energy in the lower zones (as low as 10.0 ± 2.0 J), highlighting an increased susceptibility to brittle fracture in areas with higher hardness. Following the implementation of these corrective actions—standardizing the thermal treatment to avoid excessive hardness and optimizing the internal finish via gun drilling—the modified mandrels were reintroduced into production. Mandrel service life was successfully restored to its historical level of approximately 250 pressings, thereby confirming the effectiveness of the measures adopted through the synergy of improved surface quality and optimized microstructural toughness.

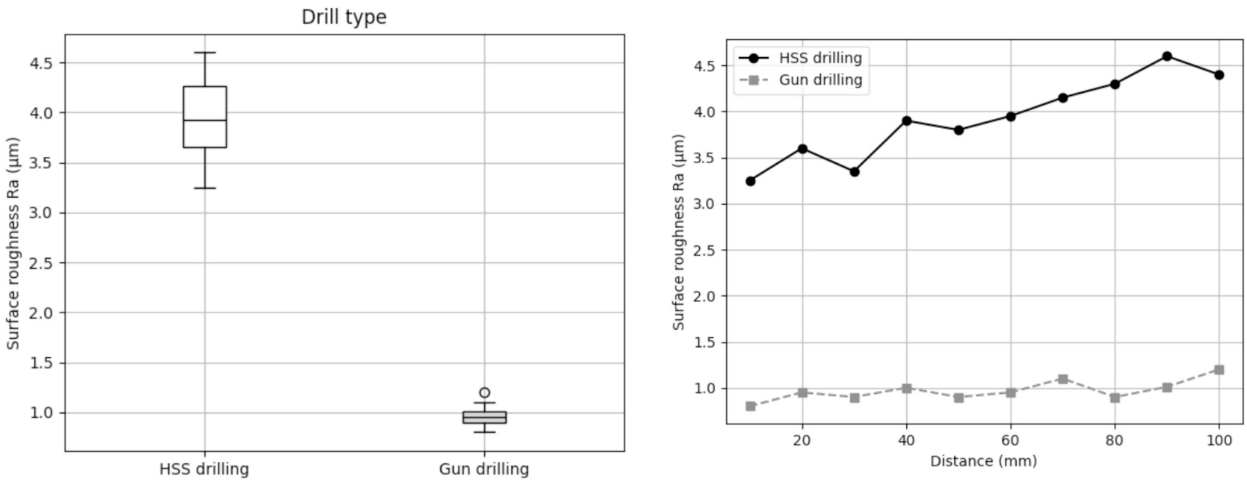

Fig. 8. Ra values obtained with the two drilling processes (HSS twist drilling vs. gun drilling).

5. Conclusions

This study investigated the premature brittle fracture of mandrels used in the hot extrusion of brass tubes through an integrated approach that combined mechanical characterization, fractographic analysis, and finite-element simulations. The main conclusions are as follows:

- Mechanical testing revealed that the mandrel material exhibits lower-than-expected toughness for the imposed service conditions. This limitation is further exacerbated by mechanical heterogeneity between the upper and lower regions, with the transition zone coinciding with the observed fracture locations.
- Fractographic analysis identified crack initiation at the cooling-channel bore. When coupled with the reduced material toughness and the poor internal surface finish produced by conventional multi-pass HSS drilling, this finding indicates that drilling-induced surface damage acted as a critical stress concentrator.
- FEM simulations predicted elevated axial tensile stresses at the cooling-channel bore during extrusion. The spatial coincidence between this high-stress region and the experimentally identified crack origin strongly supports the proposed failure mechanism.
- The replacement of conventional HSS drilling with carbide-tipped gun drilling significantly improved internal surface quality and eliminated critical surface defects. Following implementation of this corrective measure, mandrel service life was restored to the historical benchmark of approximately 250 pressings.

Three improvement routes are proposed for future assessment: (i) if cooling performance is not compromised, reduce cooling-channel diameter to decrease stress levels; (ii) further improve internal finish over $\sim$ 250 mm from the support face using ball burnishing, which can reduce roughness and increase surface hardness, thereby improving fatigue resistance [30]; and (iii) reduce the die angle from the current 90° to lower extrusion loads and mandrel stresses.

CRediT authorship contribution statement

M. Schmidt: Methodology, Investigation, Formal analysis, Data curation, Conceptualization. **D. Migliorino:** . **L. Buglioni:** Supervision, Investigation, Conceptualization. **G. Abate:** Project administration, Formal analysis. **D.Martínez Krahmer:** Supervision, Methodology, Data curation. **L.N.López de Lacalle:** Validation, Supervision, Conceptualization. **A.Sánchez Egea:** Resources, Investigation.

Declaration of competing interest

The authors declare that they have no known competing financial interests or personal relationships that could have appeared to influence the work reported in this paper.

Acknowledgements

The authors acknowledge Labtesa for the tests performed and Eng. Raniero Zambelli (INTI-Mecánica) and Mikel Abasolo (University of the Basque Country) for contributions regarding the observed fracture surfaces. Also, thanks are addressed to the Basque Government by grant to Excellence university groups: IT1894-26

Data availability

Data will be made available on request.

References

[1] H. Valberg, Applied metal forming: including FEM analysis, Cambridge University Press, 2010.
[2] G. Rowe, Principles of Industrial Metalworking Processes, 2nd ed., Edward Arnold, 1977.
[3] A. Irisarri, A. Pelayo, Failure analysis of an open die forging drop hammer, Eng. Fail. Anal. 16 (5) (2009) 1727–1733, https://doi.org/10.1016/j.engfailanal.2008.12.
[4] D. Leśniak, J. Zasadziński, W. Libura, et al., Latest advances in extrusion processes of light metals, Arch. Civ. Mech. Eng. 24 (2024) 184, https://doi.org/10.1007/s43452-024-00988-5.
[5] S. Qamar, T. Pervez, J. Chekotu, Die defects and die corrections in metal extrusion, Metals 8 (6) (2018) 380, https://doi.org/10.3390/met8060380.
[6] M. Schwartz, G. Doncean, R. Ciocoiu, Failure of an Inconel 718 die used in production of hot copper direct extrusion, J. Mater. Sci. Eng 4 (2015), https://doi.org/10.4172/2169-0022.1000205.
[7] M. Schwartz, G. Doncean, R. Ciocoiu, I. Ciuca, Die failures in copper hot extrusion, Adv. Mater. Res. 1114 (2015) 56–61, https://doi.org/10.4028/www.scientific.net/AMR.1114.56.
[8] A. Arif, A. Sheikh, S. Qamar, A study of die failure mechanisms in aluminum extrusion, J. Mater. Process. Technol. 134 (3) (2003) 318–328, https://doi.org/10.1016/S0924-0136(02)01116-0.
[9] B. Behrens, T. Yilkiran, Influence of the fabrication method on the wear resistance of hot forging dies, Prod. Eng. Res. Devel. 6 (2012) 267–276, https://doi.org/10.1007/s11740-012-0373-y.
[10] D. Tseronis, I. Sideris, C. Medrea, I. Chicinas, Microscopic examination of the fracture surfaces of an H13 hot extrusion die due to failure at the initial usage stage, Key Eng. Mater. 367 (2008) 177–184, https://doi.org/10.4028/www.scientific.net/KEM.367.177.
[11] Z. Gasem, Cracking in a multiple gas-nitrided H13 aluminum extrusion mandrel, Eng. Fail. Anal. 31 (2013) 68–75, https://doi.org/10.1016/j.engfailanal.2013.01.
[12] L. Zhao, K. Zhou, D. Tang, et al., Experimental and numerical study on friction and wear performance of hot extrusion die materials, Materials 15 (2022) 1798, https://doi.org/10.3390/ma15051798.
[13] A. Thewes, P. Reinders, H. Paschke, et al., Surface modifications to reduce wear in hot extrusion of copper, Wear 548–549 (2024) 205358, https://doi.org/10.1016/j.wear.2024.205358.
[14] Z. Liu, M. Zhang, P. Yan, et al., Tribological characteristics of Al-Mg-Si-Cu alloy against die steel under elevated temperatures in simulated hot extrusion environment, J. Mater. Res. Technol. 34 (2024), https://doi.org/10.1016/j.jmrt.2024.12.073.
[15] S. Akhtar, A. Arif, Fatigue failure of extrusion dies: effect of process parameters and design features on die life, J. Fail. Anal. Prev. 10 (1) (2010) 38–49, https://doi.org/10.1007/s11668-009-9304-4.
[16] J. Gattmah, F. Ozturk, S. Orhan, Effects of process parameters on hot extrusion of hollow tube, Arab. J. Sci. Eng. 42 (5) (2017) 2021–2030, https://doi.org/10.1007/s13369-017-2434-1.
[17] Y. Jing, H. Rufu, Closed-die forging process of copper alloy valve body: finite element simulation and experiments, J. Mater. Res. Technol. 10 (2020), https://doi.org/10.1016/j.jmrt.2020.12.087.
[18] Z. Lin, X. Juchen, W. Xinyun, H. Guoan, Optimization of die profile for improving die life in the hot extrusion process, J. Mater. Process. Technol. 142 (3) (2003) 659–664, https://doi.org/10.1016/S0924-0136(03)00686-1.
[19] A.A.K. Ahmed, M. Ibrahim, A. Ibrahim, M.A. Allow, Improvement of forging die life by failure mechanism analysis, J. Mech. Behav. Mater. 30 (1) (2021) 309–317, https://doi.org/10.1515/jmbm-2021-0034.
[20] K. Srinivasan, P. Venugopal, Influence of die angle on containerless extrusion of commercially pure titanium tubes, Mater. Manuf. Process. 22 (2) (2007) 238–242, https://doi.org/10.1080/10426910601134047.
[21] M. Hawryluk, M. Lachowicz, M. Janik, et al., Influence of the nitrided layer thickness of dies made of two types of tool steel used in hot extrusion of valve forgings made of nickel–chromium steel on durability, Arch. Civ. Mech. Eng. 21 (2021) 151, https://doi.org/10.1007/s43452-021-00301-8.
[22] Q. He, G.K. Dosbaeva, Microstructural evaluation and failure analysis of flow forming mandrels: Case studies, Eng. Fail. Anal. 184 (2026), https://doi.org/10.1016/j.engfailanal.2025.110322.
[23] S.S.M. Tavares, H.L.A. Keide, P.S.P. Garcia, J.A.C. Velasco, J.M. Pardal, I.P. Baptista, Intergranular corrosion at a modified surface layer in a supermartensitic stainless steel for chemical injection mandrel, Eng. Fail. Anal. 125 (2021), https://doi.org/10.1016/j.engfailanal.2021.105390.
[24] N. Wilda, J. Giedenbacher, A. Huskic, Material properties of AISI H10 (32CrMoV12-28) hot work tool steel processed by Laser Powder Bed Fusion with 200°C substrate preheating temperature, Procedia Computer Science, volume 217, ISSN 1008–1017 (2023) 1877–10509, https://doi.org/10.1016/j.procs.2022.12.299.
[25] F. Klocke, Manufacturing Processes 2: Grinding, Honing, Springer, Lapping, 2009.
[26] S. Qamar, Heat treatment and mechanical testing of AISI H11 steel, Key Eng. Mater. 656–657 (2015) 434–439, https://doi.org/10.4028/www.scientific.net/KEM.656-657.434.
[27] Arsic D, Lazic V, Nikolic R (2018). Mechanical properties of hot-work tool steel at elevated temperatures.
[28] M. Aamir, A. Sharif, M. Zahir, K. Giasin, M. Tolouei-Rad, Experimental assessment of hole quality and tool condition in the machining of an aerospace alloy, Machines 11 (2023) 726, https://doi.org/10.3390/machines11070726.
[29] D. Neo, K. Liu, A. Kumar, High throughput deep-hole drilling of Inconel 718 using PCBN gun drill, J. Manuf. Process. 57 (2020) 302–311, https://doi.org/10.1016/j.jmapro.2020.06.043.
[30] A. Rodriguez, L.N.L. de Lacalle, O. Pereira, et al., Isotropic finishing of austempered iron casting cylindrical parts by roller burnishing, Int. J. Adv. Manuf. Technol. 110 (2020) 753–761, https://doi.org/10.1007/s00170-020-05894-7.